

## Studies of the Colloidal Properties of Superparamagnetic Iron Oxide Nanoparticles Functionalized with Platinum Complexes in Aqueous and PBS Buffer Media

*Gustavo B. da Silva,<sup>a,b</sup> Marzia Marciello,<sup>b</sup> María del Puerto Morales,<sup>b</sup> Carlos J. Serna,<sup>b</sup> Maria D. Vargas,<sup>\*a</sup> Célia M. Ronconi<sup>\*a</sup> and Rocío Costo<sup>b</sup>*

<sup>a</sup>*Instituto de Química, Universidade Federal Fluminense, Campus do Valonguinho, Outeiro São João Batista s/n, Centro, 24020-150 Niterói-RJ, Brazil*

<sup>b</sup>*Departamento de Biomateriales y Materiales Bioinspirados, Instituto de Ciencia de Materiales de Madrid (ICMM)/CSIC, Sor Juana Inés de la Cruz 3, Cantoblanco 28049 Madrid, Spain*

This work has focused on the synthesis of three nanosystems composed of superparamagnetic iron oxide nanoparticles (SPIONs) coated either with a carboxylate platinum(IV) complex (PD = *cis,cis,trans*-[Pt(NH<sub>3</sub>)<sub>2</sub>Cl<sub>2</sub>(HOOCCH<sub>2</sub>CH<sub>2</sub>COO)(OH)]) or with platinum(II) complex functionalized dextrans (DexPt1 = [Pt(Dex-NH<sub>2</sub>)Cl<sub>3</sub>] and DexPt2 = [Pt(Dex-NH<sub>2</sub>)(NH<sub>3</sub>)<sub>2</sub>(H<sub>2</sub>O)]). All nanosystems have shown superparamagnetic behavior. Powder X-ray diffraction (XRD) has confirmed that the SPIONs were iron oxide phase and transmission electron microscopy (TEM) has shown average size of 6 nm (M6). Characterization of the nanosystems by inductively coupled plasma atomic emission spectroscopy (ICP AES) has revealed the presence of platinum on their surface (M6@PD, 0.54 mmol g<sup>-1</sup> of Fe and M6@CA@DexPt1-2, 0.32-1.20 mmol g<sup>-1</sup> of Fe); infrared spectroscopy (IR) and thermogravimetric and differential thermal analyses (TG-DTA) have confirmed the presence of dextran. Furthermore, the colloidal properties of these nanosystems (M6@PD and M6@CA@DexPt1-2) have been evaluated in water and in PBS buffer. Although M6@PD has shown good colloidal dispersion in water in the pH range of 2.0-8.0, the system underwent rapid agglomeration in PBS buffer. The M6@CA@DexPt1-2 nanosystems have exhibited improved colloidal behavior both in water and in PBS, where hydrodynamic sizes were kept below 100 nm over a large pH range (2.0-12.0). Furthermore, the latter systems have displayed isoelectric points below pH 5.0 and low surface charges at pH 7.0 ( $\zeta$ -potential = -10 mV) and therefore PBS did not affect their colloidal stability.

**Keywords:** colloidal stability, dextran, iron oxide, platinum complexes, superparamagnetism

### Introduction

Superparamagnetic iron oxide nanoparticles (SPIONs) have been widely investigated for biomedical purposes.<sup>1</sup> Magnetic resonance imaging,<sup>2-4</sup> hyperthermia<sup>5-7</sup> and drug delivery<sup>8-12</sup> are some of the practical applications displayed by SPIONs. These nanomaterials are promising due to the biocompatibility of the iron oxide cores, e.g., magnetite (Fe<sub>3</sub>O<sub>4</sub>) and maghemite ( $\gamma$ -Fe<sub>2</sub>O<sub>3</sub>).<sup>13</sup> Furthermore, their surfaces can be easily modified, allowing for the tuning of pharmacokinetic properties.<sup>14-16</sup>

One of the key features for biomedical applications of SPIONs is their aqueous colloidal stability.<sup>17</sup> Therefore, surface functionalization plays a relevant role on the balance of attractive forces, such as dispersion

forces and dipole-dipole interactions that determine their agglomeration.<sup>18</sup> Carboxylate-, phosphonate- and aminosilane-based derivatives have been widely used to coat SPIONs in order to prevent aggregation, mainly by electrostatic interactions due to the formation of an electrical double layer.<sup>16-19</sup> However, this kind of colloidal dispersion is strongly affected by physiological pH and ionic strength.<sup>17</sup> Coating nanoparticles with polymers, such as dextran (Dex) or poly(ethylene glycol) (PEG), is a judicious strategy to prevent SPIONs from aggregation,<sup>13,20</sup> diminishing opsonization and increasing circulation time.<sup>21</sup> These polymers can be adsorbed or chemically attached onto the surface of SPIONs, and because the stabilization of these systems is due to steric repulsions, they are less affected by pH and ionic strength changes than SPIONs modified via electrostatic interactions.<sup>17</sup> Nonetheless the colloidal stability of these systems under physiological

\*e-mail: mdvargas@vm.uff.br; cmronconi@id.uff.br

conditions must be thoroughly investigated before any further *in vitro* or *in vivo* studies.

Coating SPIONs with dextran has led to improvement of their colloidal stability.<sup>18</sup> Impregnation of cisplatin in the dextran-coated SPIONs has been investigated for the delivery of this drug to cancer cells.<sup>22</sup> However, the drug could be released prematurely before reaching its target. Thus, the use of SPIONs coated with dextran modified with platinum(II) complexes may circumvent this problem. In this work we report the use of two new strategies (Scheme 1) to attach platinum complexes onto the surface of 6 nm SPIONs (M6): (i) by coating the SPIONs with platinum(II) complex functionalized dextran (DexPt1-2) and (ii) by direct coordination of a carboxylate platinum(IV) complex (PD) for comparison. Furthermore, the colloidal properties of these nanosystems (M6@CA@DexPt1-2 and M6@PD) have been evaluated in aqueous and PBS buffer media. These studies are essential to comprehend their behavior, especially with respect to aggregation and surface charge, which will dictate their future applications.

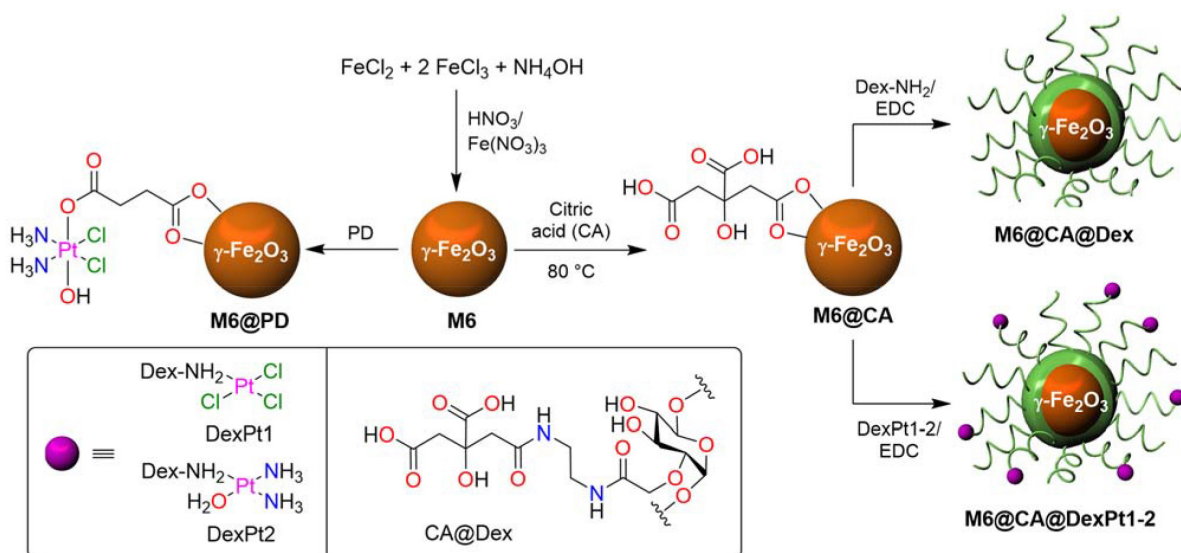
## Experimental

### Materials and methods

Carboxymethyl-dextran sodium salt (CM-Dex), citric acid (CA,  $\geq 99.5\%$ ), *N*-ethyl-*N'*-(3-dimethylaminopropyl) carbodiimide hydrochloride (EDC,  $\geq 99\%$ ), ethylenediamine (EDA,  $\geq 99\%$ ), hydrochloric acid ( $\geq 36\%$ ), hydrogen peroxide solution (30%), iron(II) chloride ( $\geq 99\%$ ), iron(III) nitrate ( $\geq 98\%$ ), nitric acid ( $\geq 65\%$ ), PBS buffer, potassium chloride ( $\geq 99\%$ ), potassium hydroxide ( $\geq 85\%$ ), potassium iodide ( $\geq 99\%$ ), potassium tetrachloroplatinate(II) (98%),

silver nitrate ( $\geq 99\%$ ), succinic anhydride ( $\geq 99\%$ ) and all necessary solvents were purchased from Sigma-Aldrich. Ammonium hydroxide solution (25%) was purchased from Fluka. Iron(III) chloride aqueous solution (27%) was purchased from VWR International. All reagents and solvents were used as received.

A Bruker (USA) D8 Advance powder diffractometer by using the CuK $\alpha$  radiation ( $\lambda = 1.5418 \text{ \AA}$ ) with an energy-discriminator (Sol-X) detector was used to identify the crystal structure of the synthesized magnetic nanoparticles and the pattern were collected within  $5^\circ$  and  $90^\circ$  in  $2\theta$ . The core size of the nanoparticles was determined from transmission electron microscopy (TEM) micrographs using 200 keV JEOL-2000 FXII and 100 keV JEOL JEM1010 microscopes. The particles were dispersed in ethanol or water and a drop of the suspension was placed onto a copper grid covered by a carbon film. The average particle sizes and their distributions were evaluated by measuring the largest internal dimension of at least 100 particles. The data were fitted to a log normal distribution by obtaining the mean size and the standard deviation ( $\sigma$ ). A PerkinElmer (USA) OPTIMA 2100DV ICP AES apparatus was used to measure the concentration of iron and platinum in compounds after acid digestion, which was carried out with 0.5-1.0 mL of 12 mol L<sup>-1</sup> HCl (for iron) and a mixture of 3:1 of 12 mol L<sup>-1</sup> HCl + 15 mol L<sup>-1</sup> HNO<sub>3</sub> (for platinum), added to the samples (25-50  $\mu$ L), which were stirred for 5 min, and then, diluted to 25-50 mL with deionized water. The infrared (IR) spectra were acquired in a Bruker (USA) IFS 66 V-S equipment. Samples were diluted in 2% potassium bromide and recorded between 4000 and 250 cm<sup>-1</sup>. Simultaneous measurements of thermogravimetric and differential



**Scheme 1.** Design of nanosystems functionalized with platinum complexes.

thermal analyses (TG-DTA) were performed on a Seiko TG/DTA 320U thermobalance (Seiko Instruments) to determine the percentage of coating molecules on the surface of nanoparticles. Samples were placed in alumina crucibles and heated from room temperature to 900 °C at 10 °C min<sup>-1</sup> under an air flow of 100 mL min<sup>-1</sup>. The magnetic characterization of the samples was recorded in a vibrating sample magnetometer (MLVSM9, MagLab 9T, VSM, Oxford Instrument). For the measurement of powders, the samples were freeze-dried for 24 h in a LyoQuest freeze dryer (Telstar). The samples were accurately weighed and fitted into gelatin capsules for magnetic measurements. For the measurement of liquids, 100 µL of the sample were placed in a small piece of cotton, dried and fitted into gelatin capsules. The temperature was kept under 250 K. Hysteresis loops of the powdered samples were measured at room temperature and at 5 K at a rate of 5 kOe min<sup>-1</sup>.

#### Synthesis of platinum-based and platinum(II) complex functionalized dextran precursors

Cisplatin (*cis*-[Pt(NH<sub>3</sub>)<sub>2</sub>Cl<sub>2</sub>]),<sup>23</sup> *cis*-[Pt(NH<sub>3</sub>)<sub>2</sub>I<sub>2</sub>],<sup>23</sup> oxoplatin (*cis,cis,trans*-[Pt(NH<sub>3</sub>)<sub>2</sub>Cl<sub>2</sub>(OH)<sub>2</sub>])<sup>24</sup> and the platinum(IV) complex PD (*cis,cis,trans*-[Pt(NH<sub>3</sub>)<sub>2</sub>Cl<sub>2</sub>(HOOCCH<sub>2</sub>CH<sub>2</sub>COO)(OH)])<sup>24</sup> were synthesized according to the literature and their identity, confirmed by melting point measurements and <sup>1</sup>H and <sup>195</sup>Pt nuclear magnetic resonance (NMR) spectra.

For the synthesis of platinum(II) complex functionalized dextran-coated nanoparticles, CM-Dex was first chemically modified with 1 mol L<sup>-1</sup> EDA (pH 4.75).<sup>25</sup> Briefly, 160 mL of this solution were added to 16 g of CM-Dex and stirred. After adjusting the pH to 4.75, EDC (0.32 g) was added and once again the pH was adjusted to 4.75. The solution was kept under stirring for 12 h and then, purified by dialysis using a membrane with a 12,000-14,000 nominal molecular weight cut off. This procedure afforded an amino-modified dextran (Dex-NH<sub>2</sub>) solution with an estimated concentration of modified/unmodified dextran of 0.04 g mL<sup>-1</sup>, which was further modified with platinum derivatives as follows. A sample of this solution was freeze-dried for analysis that showed 14% of functionalized polymer molecules: anal. calcd. for [(C<sub>8</sub>H<sub>12</sub>O<sub>7</sub>)<sub>6</sub>(C<sub>10</sub>H<sub>18</sub>N<sub>2</sub>O<sub>6</sub>)<sub>6</sub>].12H<sub>2</sub>O: C 38.71, H 6.39, N 1.56%. Found: C 39.57, H 6.37, N 1.52%. Fourier transform infrared spectroscopy (FTIR) (KBr)  $\nu_{\max}$  / cm<sup>-1</sup>: 3434 (O–H), 2924 (C–H), 1595 (C=O),<sup>20</sup> 1280, 1156, 1016 (C–O) and 915, 845 (C–C).

#### K[Pt(Dex-NH<sub>2</sub>)Cl<sub>3</sub>] (DexPt1)

Potassium tetrachloroplatinate(II) (0.137 g, 0.33 mmol) was added to 30 mL of the Dex-NH<sub>2</sub> solution at pH ca. 7.

The light-red solution was stirred for 72 h. This reaction afforded a light yellow solution, which was purified by dialysis, using a membrane with a 12,000-14,000 nominal molecular weight cut off. The estimated concentration of the modified/unmodified dextran polymer was 24 mg mL<sup>-1</sup> and the quantity of platinum complex was 71 µmol g<sup>-1</sup> of dextran polymer. FTIR (KBr)  $\nu_{\max}$  / cm<sup>-1</sup>: 3417 (O–H), 3265 (N–H, shoulder), 2927 (C–H), 1598 (C=O),<sup>20</sup> 1278, 1156, 1022 (C–O) and 916, 850 (C–C).

#### [Pt(NH<sub>3</sub>)<sub>2</sub>(Dex-NH<sub>2</sub>)(H<sub>2</sub>O)](NO<sub>3</sub>)<sub>2</sub> (DexPt2)

To *cis*-[Pt(NH<sub>3</sub>)<sub>2</sub>I<sub>2</sub>] (0.484 g, 1.0 mmol) in dimethylformamide (DMF, 5 mL), silver nitrate (0.334 g, 1.98 mmol) was added as a solid and the mixture was kept in the dark for 24 h, under stirring.<sup>26</sup> The pale yellow suspension was centrifuged and the supernatant filtered through a 0.45 µm diameter porous filter. Evaporation of the solvent under vacuum yielded a dark-yellow residue of *cis*-[Pt(NH<sub>3</sub>)<sub>2</sub>(DMF)<sub>2</sub>](NO<sub>3</sub>)<sub>2</sub>. Then, 25 mL of a previously prepared Dex-NH<sub>2</sub> solution at pH ca. 7 were added to *cis*-[Pt(NH<sub>3</sub>)<sub>2</sub>(DMF)<sub>2</sub>](NO<sub>3</sub>)<sub>2</sub> and the mixture, stirred for 72 h. Finally, the pale yellow solution was filtered and purified by dialysis using a membrane with a 12,000-14,000 nominal molecular weight cut off. The estimated concentration of the modified/unmodified dextran polymer was 30 mg mL<sup>-1</sup> and the quantity of platinum complex was 318 µmol g<sup>-1</sup> of dextran polymer. FTIR (KBr)  $\nu_{\max}$  / cm<sup>-1</sup>: 3434 (O–H), 3277 (N–H, shoulder), 2927 (C–H), 1591 (C=O),<sup>20</sup> 1276, 1156, 1014 (C–O) and 913, 847 (C–C).

#### Synthesis of superparamagnetic nanoparticles M6

The preparation of maghemite nanoparticles M6 was recently reported in the literature.<sup>17</sup> These particles have been obtained in aqueous medium, following a modified Massart procedure.<sup>27,28</sup> Briefly, 75 mL of a 25% NH<sub>3</sub> aqueous solution was rapidly added to a solution containing 488 mL of 0.334 mol L<sup>-1</sup> FeCl<sub>3</sub> and 0.175 mol L<sup>-1</sup> FeCl<sub>2</sub>, under vigorous stirring and at room temperature. The particles were isolated by magnetic decantation after 5 min and washed three times with distilled water. They were then treated with HNO<sub>3</sub>/Fe(NO<sub>3</sub>)<sub>3</sub> to fully oxidize magnetite (Fe<sub>3</sub>O<sub>4</sub>) to maghemite (γ-Fe<sub>2</sub>O<sub>3</sub>), which is more biocompatible,<sup>29</sup> by adding 300 mL of 2 mol L<sup>-1</sup> HNO<sub>3</sub>, and kept under stirring. After 15 min, the supernatant was completely removed and 75 mL of 1 mol L<sup>-1</sup> Fe(NO<sub>3</sub>)<sub>3</sub> were added, followed by 130 mL of distilled water. The suspension was refluxed for 30 min and cooled to room temperature. The supernatant was removed, 300 mL of 2 mol L<sup>-1</sup> HNO<sub>3</sub> were added and the dispersion, stirred for 15 min. Finally, particles were isolated by magnetic

decantation, washed three times with acetone, and redispersed in water. The acetone residue was removed under vacuum.

#### Coating of M6 nanoparticles with citric acid (M6@CA)

A slightly modified procedure was used to prepare M6 nanoparticles coated with citric acid.<sup>19,30</sup> After addition of 80 mL of a 0.1 mol L<sup>-1</sup> citric acid solution to an aqueous dispersion of 50 mL of M6 ([Fe] ca. 15 mg mL<sup>-1</sup>), at pH 3.0, the suspension was heated at 80 °C for 30 min under mechanical stirring. The particles were isolated by centrifugation and redispersed in distilled water. The dispersion was dialyzed using a membrane with a 12,000-14,000 nominal molecular weight cut off. Finally, the pH of the M6@CA dispersion was adjusted to 7.0.

#### Coating of M6@CA nanoparticles with Dex-NH<sub>2</sub> (M6@CA@Dex)<sup>20</sup>

To a solution of 10 mL of M6@CA ([Fe] ca. 7 mg mL<sup>-1</sup>) at pH 7.0, under sonication, were slowly added 90 mL of a neutral solution of Dex-NH<sub>2</sub> ([Dex] ca. 0.04 g mL<sup>-1</sup>). EDC (0.383 g) was added, the pH adjusted to 7.0 and the solution was stirred for 12 h. The particles were then isolated by centrifugation and redispersed in distilled water. Finally, the M6@CA@Dex particles were purified by dialysis using a membrane with a 50,000 nominal molecular weight cut off.

#### Attachment of the PD onto the surface of M6 nanoparticles (M6@PD)

Briefly, to a solution of 25 mL of maghemite M6 ([Fe] ca. 15 mg mL<sup>-1</sup>) under sonication was slowly added a suspension of the PD (1 mmol in 60 mL of distilled water). The mixture was heated for 4 h at 80 °C, under mechanical stirring. The particles were isolated by centrifugation and magnetic decantation and then, redispersed in distilled water and purified by dialysis using a membrane of 12,000-14,000 nominal molecular weight cut off. Finally, the pH of the M6@PD dispersion was adjusted to 7.0.

#### Attachment of platinum(II) complex functionalized dextran derivatives to citrate-coated nanoparticles

General procedure: to a solution of 5 mL of M6@CA ([Fe] ca. 7 mg mL<sup>-1</sup>) at pH 7.0, under sonication, was slowly added 55 mL of a neutral solution of DexPt1 ([Dex] ca. 20 mg mL<sup>-1</sup>) or DexPt2 ([Dex] ca. 16 mg mL<sup>-1</sup>). The EDC (0.23 g) was added, the pH adjusted to 7.0 and the solution, stirred for 12 h. The particles were then isolated by centrifugation and redispersed in distilled water. Finally, the M6@CA@DexPt1 and M6@CA@DexPt2 particles were purified by dialysis using a membrane with a 50,000 nominal molecular weight cut off.

#### Evaluation of the colloidal properties

A Zetasizer nano ZS equipment by Malvern Instruments was used to measure both the hydrodynamic diameter ( $D_H$ , obtained by Z-average size values in the dynamic light scattering measurements) and the  $\zeta$ -potential. The  $D_H$  measurements were carried out in water and performed in a large range of pH values (2.0-12.0), as well as in the presence of PBS buffer. Furthermore,  $\zeta$ -potential measurements were carried out using KNO<sub>3</sub> 0.01 mol L<sup>-1</sup> as the background electrolyte, and the isoelectric point (IEP) of nanoparticles were determined after measurements in a large range of pH values (2.0-12.0). HNO<sub>3</sub> and KOH were used to change the pH of the dispersions.

The aggregation kinetics was evaluated using a Turbiscan Lab apparatus by Formulacion. In this equipment, a laser passes through the sample and the results are reported in transmittance (%). Thus, high transmittance values indicate that the sample undergoes rapid destabilization, followed by decantation. Measurements were performed placing 20 mL of the sample ([Fe] ca. 1.0 mg mL<sup>-1</sup>) in a sample holder and collecting data along 72 h. The experiments were carried out in water and in the presence of PBS buffer at pH 7.4, at different concentrations.

## Results and Discussion

### Synthesis and general characterization

The platinum(II) complex functionalized dextran precursors were synthesized by complexation of the amino-modified dextran (Dex-NH<sub>2</sub>) with K<sub>2</sub>PtCl<sub>4</sub> and *cis*-[Pt(NH<sub>3</sub>)<sub>2</sub>I<sub>2</sub>], affording K[Pt(Dex-NH<sub>2</sub>)Cl<sub>3</sub>] (DexPt1) and [Pt(NH<sub>3</sub>)<sub>2</sub>(Dex-NH<sub>2</sub>)(H<sub>2</sub>O)](NO<sub>3</sub>)<sub>2</sub> (DexPt2), respectively. The compounds were purified by dialysis for 5-7 days; their identity was confirmed by FTIR data (see Experimental section) and the amount of platinum, determined by inductively coupled plasma atomic emission spectroscopy (ICP AES) analyses. Due to the low concentration of platinum in the samples the <sup>195</sup>Pt NMR spectra could not be obtained and <sup>1</sup>H NMR spectra of Dex-NH<sub>2</sub> and DexPt1-2 do not show appreciable differences.

Iron oxide nanoparticles ( $\gamma$ -Fe<sub>2</sub>O<sub>3</sub>, M6) were prepared by acid treatment of magnetite particles (Fe<sub>3</sub>O<sub>4</sub>), obtained by a modified Massart method.<sup>18,27,29</sup> This procedure leads to the oxidation of the Fe<sub>3</sub>O<sub>4</sub> core into  $\gamma$ -Fe<sub>2</sub>O<sub>3</sub>, activating the nanoparticles surface and thus improving their colloidal properties.<sup>29</sup> The  $\gamma$ -Fe<sub>2</sub>O<sub>3</sub> nanoparticles are more stable than Fe<sub>3</sub>O<sub>4</sub> and have been approved by the FDA (Food and Drug Administration, USA) for *in vivo* applications.<sup>18</sup>

According to TEM images, the M6 particles exhibit spherical morphology and the particle-size distribution curve shows diameter of  $6.5 \pm 0.2$  nm (Figure 1). The identity of the iron oxide with ferrite structure was confirmed by X-ray diffraction (XRD) data (Figure S1) and indexed to an inverse spinel structure (JCPDS 34-1346, maghemite). The average crystallite size of 6 nm was calculated with the Scherrer equation using full-width at half maximum of the (311) X-ray diffraction peak. Good agreement between the XRD and TEM data is observed.

Modifications on the surface of M6 nanoparticles with citric acid (CA) and the platinum(IV) complex PD (*cis,cis,trans*-[Pt(NH<sub>3</sub>)<sub>2</sub>Cl<sub>2</sub>(HOOCCH<sub>2</sub>CH<sub>2</sub>COO)(OH)] were carried out at 80 °C, affording M6@CA and M6@PD, respectively. No significant size changes are observed after this treatment according to the particle-size distribution curves that show mean diameters of  $6.2 \pm 0.3$  nm and  $5.8 \pm 1.1$  nm for M6@CA and M6@PD, respectively (Figure 1). According to TEM images, the spherical morphology of dextran-coated nanoparticles M6@CA@Dex, M6@CA@DexPt1 and M6@CA@DexPt2 is maintained (Figure S2).

The FTIR spectra of the maghemite nanoparticles before and after the functionalizations are shown in Figures 2 and S3. Besides the characteristic maghemite  $\nu(\text{Fe-O})$  modes observed at 636-630, 584-578, 441-436

and 408-396 cm<sup>-1</sup>,<sup>29</sup> a sharp intense band at 1385 cm<sup>-1</sup>, assigned to N-O modes, is observed in the spectrum of M6, due to the presence of residual nitric acid used to oxidize the particles and adjust the pH (Figure S3).<sup>29</sup> The spectra of M6@CA and M6@PD exhibit bands at 1258-1256 and 1065-1040 cm<sup>-1</sup> attributed to the vibrations of carboxylic and methylene groups, respectively.<sup>19</sup> FTIR data also confirmed the attachment of amino-modified dextran (Dex-NH<sub>2</sub>) and platinum(II) complex functionalized dextran (DexPt1-2) precursors onto M6@CA nanoparticles, affording the M6@CA@Dex and M6@CA@DexPt1-2 nanosystems (Figures 2, S3 and S4). They show the typical amide group  $\nu(\text{C=O-NH})$  (1604-1598 cm<sup>-1</sup>),<sup>20</sup> asymmetric CH<sub>2</sub> (2936-2923 cm<sup>-1</sup>), carboxylic group  $\nu(\text{C-O})$  (at around 1280, 1155 and 1015 cm<sup>-1</sup>) and  $\alpha$ -glucopyranose ring deformation modes (917 and 852 cm<sup>-1</sup>).<sup>20</sup> All spectra show the  $\nu(\text{O-H})$  modes at 3442-3400 and 1635-1624 cm<sup>-1</sup> indicating the presence of physi- and chemisorbed water molecules, respectively.<sup>19</sup>

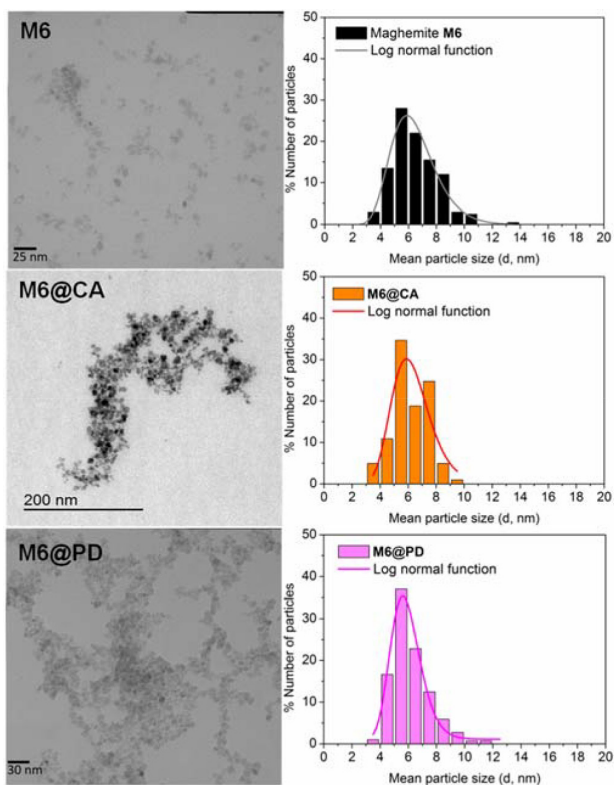


**Figure 1.** Transmission electron micrographs of M6, M6@CA and M6@PD, and particle-size distributions.

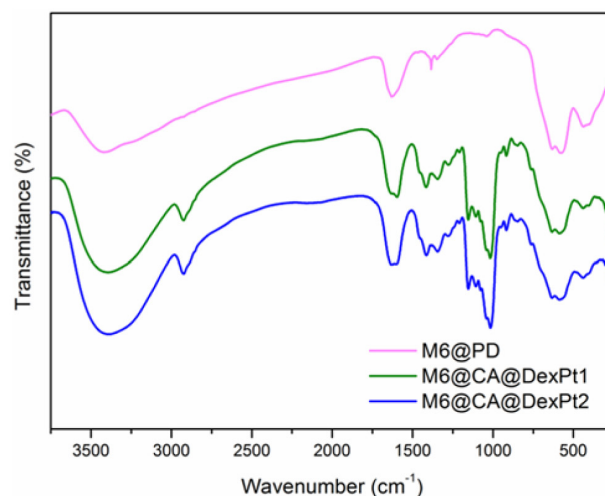


**Figure 2.** FTIR spectra of M6@PD and M6@CA@DexPt1-2 nanoparticles.

Thermal analysis (TG-DTA, Figures S5-S8) reveals the organic content of the functionalized nanoparticles. Total weight loss of 13% is observed for M6@CA nanoparticles, whereas the M6@CA@Dex, M6@CA@DexPt1 and M6@CA@DexPt2 nanosystems show 77, 66 and 62% weight losses, respectively, in one step, starting at around 150 °C, due to decomposition of the dextran coating.<sup>20</sup> These results confirm that the adopted method to attach dextran derivatives onto the surface of M6@CA is effective, affording high amounts of polymer coating.

The platinum and iron contents as well as the Pt/Fe ratios (mmol g<sup>-1</sup>) were determined by ICP AES. In the M6@PD nanomaterial, a concentration of 0.54 mmol of platinum *per* gram of iron was observed, whereas in

the M6@CA@DexPt1 and M6@CA@DexPt2 systems, 0.32 and 1.20 mmol of platinum complex *per* gram of iron were observed, respectively.

#### Evaluation of the superparamagnetic behavior

The magnetic behavior of the superparamagnetic nanosystems functionalized with platinum complexes M6@PD and M6@CA@DexPt1-2 was investigated in the solid state. Figure 3 shows the field dependence of the magnetization *per* mass of sample at 250 K. According to these data, M6@PD and the uncoated M6 nanoparticles exhibit almost the same saturation magnetization value ( $M_{\text{sat}}$  ca.  $65 \text{ emu g}^{-1}$ ), due to the low concentration of PD complex attached onto the surface of the nanoparticles.<sup>22,31</sup> Furthermore, the diamagnetic nature of the coating molecules has a negligible contribution to the magnetic properties of the samples.<sup>18,31</sup> However, the effect of the dextran coating on the magnetization of the nanoparticles is noticeable,<sup>18</sup> e.g., for M6@CA@DexPt1 a decrease of 54% on the  $M_{\text{sat}}$  was observed ( $M_{\text{sat}} = 30 \text{ emu g}^{-1}$ ). This result is related to the high amount of dextran polymer attached onto the surface of the M6 nanoparticles (according to TG-DTA data). The curves of magnetization *versus* temperature taking into account the TG-DTA results have been plotted (Figure S9). Thus, the magnetization data are reported in  $\text{emu per gram}$  of bared nanoparticles, i.e.,  $\text{emu per gram}$  of nanoparticles without organic content. At 250 K the  $M_{\text{sat}}$  values for M6, M6@PD and M6@CA@DexPt1 are 73, 76 and  $89 \text{ emu g}^{-1}$ . All systems share the same core, but the M6@PD and M6@CA@DexPt1 samples also contain platinum, which is not lost in the TG-DTA measurements.<sup>32</sup> Therefore, a comparison of these data is not direct, because the quantity of platinum is relatively high, e.g., %Pt/Fe (m/m) are 9.5 and 5.8% for M6@PD and

M6@CA@DexPt1, respectively. Thus, it is not possible to consider that the remaining mass of M6@PD and M6@CA@DexPt1 is composed only of iron oxide.

The magnetic data at 250 K indicate that M6@PD and M6@CA@DexPt1 are superparamagnetic because the coercivity ( $H_c$ ) values are zero.<sup>18</sup> The uncoated iron oxide core (M6) exhibits same behavior and this is attributed to the small size of the nanoparticles and, even after several modifications on the surface, these systems remain superparamagnetic. At low temperature (5 K, Figure 3, inset), however, M6@PD and M6@CA@DexPt1 show  $H_c$  values of 170 and 180 Oe, respectively. These similar values suggest that neither the nature nor the amount of coating material on the surface of the nanoparticles significantly affects the interparticle interactions or modify the surface layer. This result is different from previous work of our group<sup>18</sup> in which we observed that functionalizations with distinct phosphonate- and dextran-based derivatives have led to lower  $H_c$  and higher  $M_{\text{sat}}$  values when compared to the uncoated nanoparticles.

To confirm the superparamagnetic nature of the nanosystems the temperature dependence of the zero-field-cooled (ZFC) and field-cooled (FC) magnetizations was studied (Figure S10). According to ZFC/FC curves, these nanosystems show superparamagnetic behavior at room temperature. However, the blocking temperature ( $T_B$ ) determination for the M6@PD, M6@CA@DexPt1 and M6@CA@DexPt2 samples is not accurate ( $T_B$  values are between 150 and 200 K). All FC curves are flat below  $T_B$  indicating dipolar interactions even after surface modification.<sup>33</sup> Thus, the results of ZFC and FC curves suggest that the nanosystems exhibit large size distributions, as confirmed by TEM images (Figure 1).

#### Colloidal properties evaluation

The aqueous aggregate sizes of M6 nanoparticles were determined over a large range of pH values (Figure S11). At  $\text{pH} < 6.0$  the nanoparticles exhibit excellent colloidal stability and hydrodynamic diameter ( $D_H$ ) below 50 nm. At  $\text{pH} 7.0$ , however, strong destabilization is observed and associated with the isoelectric point (IEP) of these particles, as previously determined in  $0.01 \text{ mol L}^{-1} \text{ KNO}_3$ .<sup>19</sup> Moreover, same behavior was observed for the destabilization kinetics in water (Figure S12). At  $\text{pH} 7.0$ , M6 nanoparticles are unstable even in the first hour of measurement. However, at  $\text{pH} 3.0$ , the nanoparticles are stable.

Coating of these nanoparticles with the platinum(IV) complex PD to give M6@PD, with citric acid (CA)<sup>19</sup> to yield M6@CA and further with amine-modified dextran (Dex-NH<sub>2</sub>) or platinum(II) complex functionalized dextran

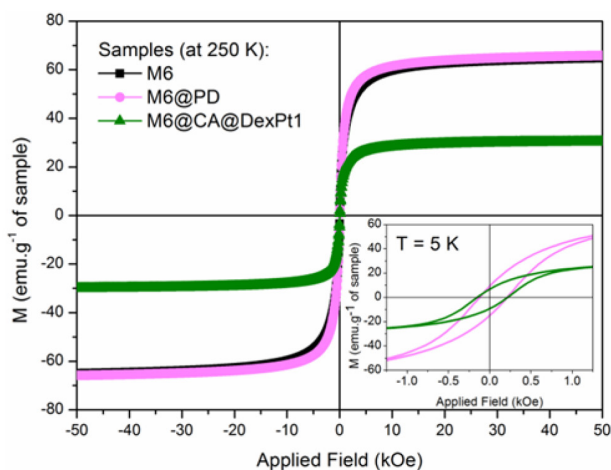


**Figure 3.** Field dependence of the magnetization ( $M$ ) measured at 250 and 5 K (inset) for M6, M6@PD and M6@CA@DexPt1.

(DexPt1 or DexPt2) to yield, respectively, M6@CA@Dex and M6@CA@DexPt1 or M6@CA@DexPt2, resulted in improved stability over a large pH range (Figures 4a-4c and S13).

PD attachment onto the surface of M6 shifts the isoelectric point (IEP) to pH 8.1, giving a surface charge of +16 mV at pH 7.0 (Figure 4a). Despite the low positive surface charge on M6@PD, the system exhibits  $D_H < 100$  nm at pH values below 8.0, which is essential for biomedical applications. Attachment of Dex-NH<sub>2</sub> and of DexPt1 and DexPt2 onto M6 shifts the IEP from pH 7.0 to 2.8, 3.6 and 2.9 for M6@CA@Dex, M6@CA@DexPt1 and M6@CA@DexPt2, respectively. These results are in agreement with the elemental analysis data that showed that only 14% of the carboxylic groups of the carboxymethyl-dextran precursor reacted with ethylenediamine (EDA, Scheme 2), thus leaving many free carboxylate groups that are able to attach onto the surface of the nanoparticles and/or to establish electrostatic interactions in aqueous medium. Furthermore, the systems exhibit very similar  $\zeta$ -potential values at pH 7.0, M6@CA@Dex ( $\zeta = -14$  mV), M6@CA@DexPt1 and M6@CA@DexPt2 (about  $\zeta = -12$  mV), because of the small amount of platinum

complex present in the latter systems. In addition, these low negative values are associated to the stabilization of the systems mainly by steric repulsions, due to the high amount of dextran polymer attached onto the nanosystems (62-77%).

Therefore, the second strategy of SPIONs coating with platinum(II) complexes functionalized dextran yielded superior results, due to a combination of electrostatic interactions and steric repulsions, in comparison with direct attachment of the carboxylate platinum(IV) complex PD, see Scheme 1. Indeed, improved aqueous stability is observed for M6@CA@DexPt1 and M6@CA@DexPt2 with  $D_H$  values below 100 nm over a large pH range (2.0-12.0) (Figures 4b, 4c and S13).

Having confirmed the stability of the nanosystems in aqueous medium, their behavior in PBS buffer was evaluated. The M6@PD nanosystem exhibits  $D_H$  of 46 nm at pH ca. 7 in water, but in PBS buffer aggregation takes place and  $D_H$  increases to 172 nm (Table 1 and Figure 5). These results are in agreement with the destabilization plots (Figures 4d and S14), confirming that in PBS buffer rapid agglomeration occurs. Interestingly, however, the M6@CA@DexPt1-2 nanosystems are unaffected by PBS

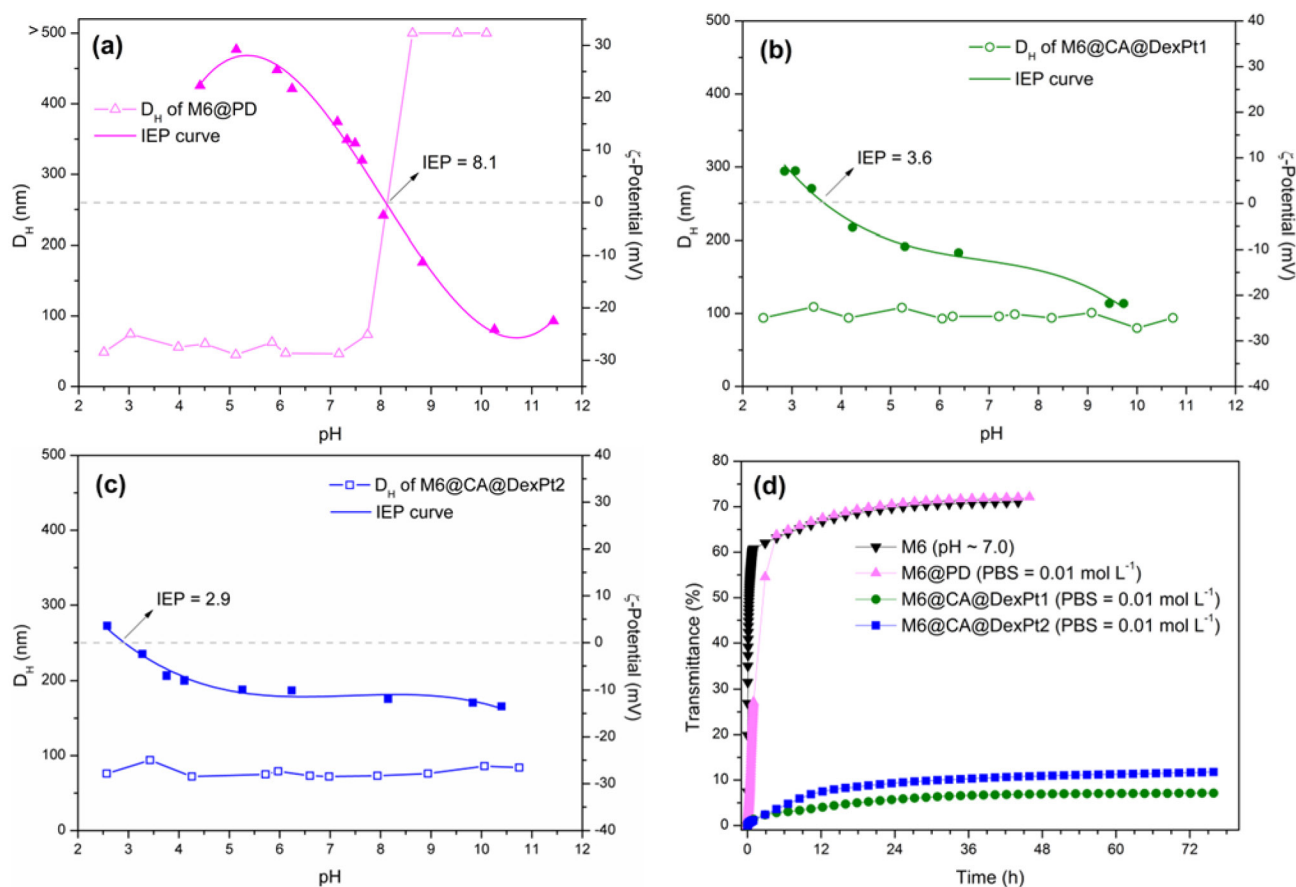
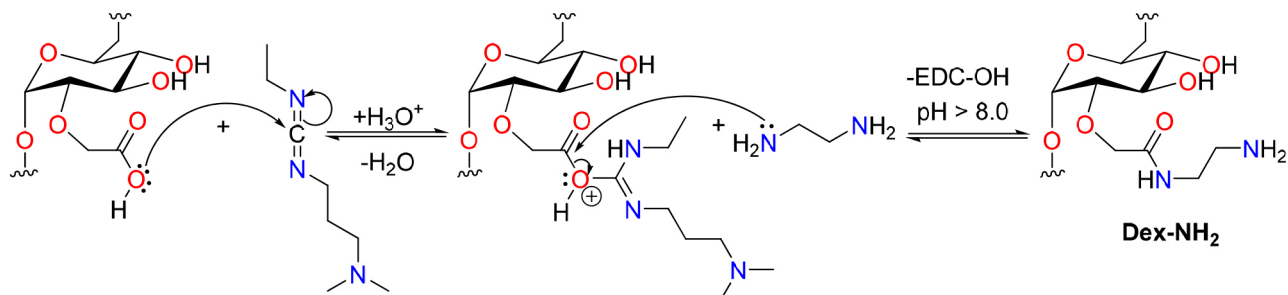


**Figure 4.** Hydrodynamic diameter ( $D_H$ ) in water and  $\zeta$ -potential *versus* pH, in 0.01 mol L<sup>-1</sup> KNO<sub>3</sub> for (a) M6@PD; (b) M6@CA@DexPt1 and (c) M6@CA@DexPt2; (d) destabilization kinetic plots of M6 in water and M6@PD and M6@CA@DexPt1-2 in 0.01 mol L<sup>-1</sup> PBS.



**Scheme 2.** Mechanistic pathway for the synthesis of the Dex-NH<sub>2</sub> precursor.

buffer. Indeed, their  $D_H$  are almost the same in water and in PBS buffer (Table 1 and Figure 5) and according to the destabilization kinetic plots (Figures 4d, S15 and S16), both nanosystems are stable over 72 h.

**Table 1.** Hydrodynamic diameters ( $D_H$ ) in water and in 0.01 mol L<sup>-1</sup> PBS buffer media

Sample	$D_H$ (pH 7.0) / nm	$D_H$ (PBS 0.01 mol L <sup>-1</sup> ) / nm
M6	> 500	N.D.
M6@PD	46	172
M6@CA@DexPt1	96	86
M6@CA@DexPt2	72	79

\* N.D. = not determined.

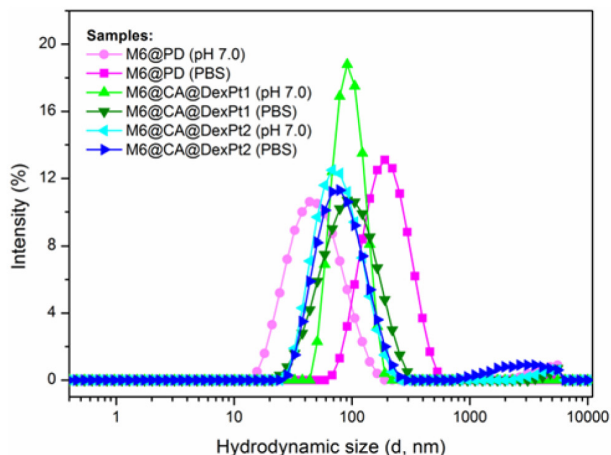


**Figure 5.** Effect of addition of 0.01 mol L<sup>-1</sup> PBS buffer on hydrodynamic diameter of nanosystems.

## Conclusions

Beyond doubt, studies of the ionic strength and the presence of phosphate anions on the colloidal stability of nanosystems is the first step in their evaluation for biomedical applications. Our results show that the attachment of platinum drugs onto the surface of small SPIONs (M6@PD) without a protective coating is not suitable because the PBS buffer fully affects ionic strength,

leading to agglomeration of the particles. The platinum(II) complex functionalized dextran-coated SPIONs (M6@CA@DexPt1-2) exhibit good dispersion properties under these conditions, without agglomeration over a large pH range (2.0-12.0). Furthermore, the use of different platinum complexes in the M6@CA@DexPt1-2 systems leads to similar colloidal properties.

## Supplementary Information

Supplementary information (thermogravimetric analyses, hydrodynamic diameter *versus* pH destabilization kinetic plots in water and in PBS buffer) is available free of charge at <http://jbcs.sbq.org.br>.

## Acknowledgments

The authors would like to thank the Brazilian agencies National Council for Scientific and Technological Development (CNPq: Jovens Pesquisadores em Nanotecnologia grant number 550572/2012-0 and G. B. da Silva was recipient of Science without borders fellowship grant number 279444/2013-9), Brazilian Federal Agency for Support and Evaluation of Graduate Education (CAPES) and Rio de Janeiro Research Foundation (FAPERJ) for financial support. M. D. Vargas and C. M. Ronconi are recipients of CNPq research fellowships. We also thank the Multiuser Laboratory of Material Characterization (<http://www.uff.br/lamate/>). R. Costo and M. P. Morales would like to thank NANOMAG project (EC FP-7 grant agreement number 604448) for funding. X-ray diffraction, FTIR spectroscopy and thermogravimetric and chemical analysis were carried out in the support laboratories of Instituto de Ciencia de Materiales de Madrid (ICMM/CSIC).

## References

- Demirer, G. S.; Okur, A. C.; Kizilel, S.; *J. Mater. Chem. B* **2015**, *3*, 7831.

2. Barick, K. C.; Singh, S.; Badahur, D.; Lawande, M. A.; Patkar, D. P.; Hassan, P. A.; *J. Colloid Interface Sci.* **2014**, *418*, 120.
3. Nafujjaman, M.; Revuri, V.; Nurunnabi, M.; Cho, K. J.; Lee, Y.; *Chem. Commun.* **2015**, *51*, 5687.
4. Zottis, A. D. A.; Beltrame, J. M.; Lara, L. R. S.; Costa, T. G.; Feldhaus, M. J.; Pedrosa, R. C.; Ourique, F.; Campos, C. E. M.; Isoppo, E. A.; Miranda, F. S.; Szpoganicz, B.; *Chem. Commun.* **2015**, *51*, 11194.
5. Di Corato, R.; Béalle, G.; Kolosnjaj-Tabi, J.; Espinosa, A.; Clément, O.; Silva, A. K. A.; Ménager, C.; Wilhelm, C.; *ACS Nano* **2015**, *9*, 2904.
6. Kakwere, H.; Leal, M. P.; Materia, M. E.; Curcio, A.; Guardia, P.; Niculaes, D.; Marotta, R.; Falqui, A.; Pellegrino, T.; *ACS Appl. Mater. Interfaces* **2015**, *7*, 10132.
7. Kossatz, S.; Grandke, J.; Couleaud, P.; Latorre, A.; Aires, A.; Crosbie-Staunton, K.; Ludwig, R.; Dähring, H.; Ettelt, V.; Lazaro-Carrillo, A.; Calero, M.; Sader, M.; Courty, J.; Volkov, Y.; Prina-Mello, A.; Villanueva, A.; Somoza, A.; Cortajarena, A. L.; Miranda, R.; Hilger, I.; *Breast Cancer Res.* **2015**, *17*, 66.
8. Hayashi, K.; Ono, K.; Suzuki, H.; Sawada, M.; Moriya, M.; Sakamoto, W.; Yogo, T.; *ACS Appl. Mater. Interfaces* **2010**, *2*, 1903.
9. Zhang, F.; Braun, G. B.; Pallaoro, A.; Zhang, Y.; Shi, Y.; Cui, D.; Moskovits, M.; Zhao, D.; Stucky, G. D.; *Nano Lett.* **2012**, *12*, 61.
10. Hsiao, M. H.; Mu, Q.; Stephen, Z. R.; Fang, C.; Zhang, M.; *ACS Macro Lett.* **2015**, *4*, 403.
11. Stephen, Z. R.; Kievit, F. M.; Veiseh, O.; Chiarelli, P. A.; Fang, C.; Wang, K.; Hatzinger, S. J.; Ellenbogen, R. G.; Silber, J. R.; Zhang, M.; *ACS Nano* **2014**, *8*, 10383.
12. Javid, A.; Ahmadian, S.; Saboury, A. A.; Kalantar, S. M.; Razaeei-Zarchi, S.; *RSC Adv.* **2014**, *4*, 13719.
13. Sun, C.; Du, K.; Fang, C.; Bhattarai, N.; Veiseh, O.; Kievit, F.; Stephen, Z.; Lee, D.; Ellenbogen, R. G.; Ratner, B.; Zhang, M.; *ACS Nano* **2010**, *4*, 2402.
14. Gupta, A. K.; Gupta, M.; *Biomaterials* **2005**, *26*, 3995.
15. Calatayud, M. P.; Sanz, B.; Raffa, V.; Riggio, C.; Ibarra, M. R.; Goya, G. F.; *Biomaterials* **2014**, *35*, 6389.
16. Calero, M.; Gutiérrez, L.; Salas, G.; Luengo, Y.; Lázaro, A.; Acedo, P.; Morales, M. P.; Miranda, R.; Villanueva, A.; *Nanomedicine* **2014**, *10*, 733.
17. Laurent, S.; Forge, D.; Port, M.; Roch, A.; Robic, C.; Elst, L. V.; Muller, R. N.; *Chem. Rev.* **2008**, *108*, 2064.
18. Costo, R.; Morales, M. P.; Veintemillas-Verdaguer, S.; *J. Appl. Phys.* **2015**, *117*, 064311.
19. Gutiérrez, L.; Romero, S.; da Silva, G. B.; Costo, R.; Vargas, M. D.; Ronconi, C. M.; Serna, C. J.; Veintemillas-Verdaguer, S.; Morales, M. P.; *Biomed. Eng. / Biomed. Tech.* **2015**, *60*, 417.
20. Marciello, M.; Connord, V.; Veintemillas-Verdaguer, S.; Vergés, M. A.; Carrey, J.; Respaud, M.; Serna, C. J.; Morales, M. P.; *J. Mater. Chem. B* **2013**, *1*, 5995.
21. Kunzmann, A.; Anderson, B.; Thurnherr, T.; Krug, H.; Scheynius, A.; Fadeel, B.; *Biochim. Biophys. Acta* **2011**, *1810*, 361.
22. Unterweger, H.; Tietze, R.; Janko, C.; Zaloga, J.; Lyer, S.; Dürr, S.; Taccardi, N.; Goudouri, O. M.; Hoppe, A.; Eberbeck, D.; Schubert, D. W.; Boccaccini, A. R.; Alexiou, C.; *Int. J. Nanomed.* **2014**, *9*, 3659.
23. Huq, F.; Daghriri, H.; Yu, J. Q.; Beale, P.; Fisher, K.; *Eur. J. Med. Chem.* **2004**, *39*, 691.
24. Shi, Y.; Liu, S. A.; Kerwood, D. J.; Goodisman, J.; Dabrowiak, J. C.; *J. Inorg. Biochem.* **2012**, *107*, 6.
25. Fernandez-Lorente, G.; Godoy, C. A.; Mendes, A. A.; Lopez-Gallego, F.; Grazu, V.; de Las Rivas, B.; Palomo, J. M.; Hermoso, J.; Fernandez-Lafuente, R.; Guisan, J. M.; *Biomacromolecules* **2008**, *9*, 2553.
26. Jawbry, S.; Freikman, I.; Najajreh, Y.; Perez, J. M.; Gibson, D.; *J. Inorg. Biochem.* **2005**, *99*, 1983.
27. Massart, R.; *IEEE Trans. Magn.* **1981**, *17*, 1247.
28. Santos, E. C. S.; dos Santos, T. C.; Guimarães, R. B.; Ishida, L.; Freitas, R. S.; Ronconi, C. M.; *RSC Adv.* **2015**, *5*, 48031.
29. Costo, R.; Bello, V.; Robic, C.; Port, M.; Marco, J. F.; Morales, M. P.; Veintemillas-Verdaguer, S.; *Langmuir* **2012**, *28*, 178.
30. Martina, M. S.; Fortin, J. P.; Ménager, C.; Clément, O.; Barratt, G.; Grabielle-Madlmont, C.; Gazeau, F.; Cabuil, V.; Lesieur, S.; *J. Am. Chem. Soc.* **2005**, *127*, 10676.
31. Huang, C.; Neoh, K. G.; Xu, L.; Kang, E. T.; Chiong, E.; *Biomacromolecules* **2012**, *13*, 2513.
32. Carvalho, M. A.; Shishido, S. M.; Souza, B. C.; de Paiva, R. E. F.; Gomes, A. F.; Gozzo, F. C.; Formiga, A. L. B.; Corbi, P. P.; *Spectrochim. Acta, Part A* **2014**, *122*, 209.
33. Guardia, P.; Battle-Brugal, B.; Roca, A. G.; Iglesias, O.; Morales, M. P.; Serna, C. J.; Labarta, A.; Battle, X.; *J. Magn. Mater.* **2007**, *316*, e756.

Submitted: April 19, 2016

Published online: August 1, 2016